Rényi Entropies from Random Quenches in Atomic Hubbard and Spin Models

A. Elben,[1,2] B. Vermersch,[1,2] M. Dalmonte,[3] J. I. Cirac,[4] and P. Zoller[1,2,4]
[1]*Institute for Theoretical Physics, University of Innsbruck, Innsbruck A-6020, Austria*
[2]*Institute for Quantum Optics and Quantum Information, Austrian Academy of Sciences, Innsbruck A-6020, Austria*
[3]*The Abdus Salam International Center for Theoretical Physics, Strada Costiera 11, 34151 Trieste, Italy*
[4]*Max-Planck-Institut für Quantenoptik, Hans-Kopfermann-Strasse 1, D-85748 Garching, Germany*

(Received 15 September 2017; published 2 February 2018)

We present a scheme for measuring Rényi entropies in generic atomic Hubbard and spin models using single copies of a quantum state and for partitions in arbitrary spatial dimensions. Our approach is based on the generation of random unitaries from random quenches, implemented using engineered time-dependent disorder potentials, and standard projective measurements, as realized by quantum gas microscopes. By analyzing the properties of the generated unitaries and the role of statistical errors, with respect to the size of the partition, we show that the protocol can be realized in existing quantum simulators and used to measure, for instance, area law scaling of entanglement in two-dimensional spin models or the entanglement growth in many-body localized systems.

DOI: 10.1103/PhysRevLett.120.050406

Atomic physics provides us with the realization of engineered quantum many-body lattice models. This includes Hubbard models for bosonic and fermionic cold atoms in optical lattices [1] and spin models with Rydberg atoms [2] and chains of trapped ions [3]. Among the noticeable recent experimental advances are quantum control and single shot measurements in lattice systems of atoms [4–11] and ions [12,13] achieving single site resolution, as illustrated for atoms in optical lattices by the quantum gas microscope [14]. This provides us not only with a unique atomic toolbox to prepare equilibrium and nonequilibrium states of quantum matter but also with the opportunity to access in experiments novel classes of observables, beyond the familiar low-order correlation functions. An outstanding example is the measurement of Rényi entropies, defined as $S^{(n)}(\rho_A) = [1/(1-n)]\log \mathrm{Tr}(\rho_A^n)$ $(n > 1)$ with $\rho_A = \mathrm{Tr}_{\mathcal{S}\setminus A}[\rho]$ the reduced density matrix of a subsystem $A \subset \mathcal{S}$ of a many-body system $\mathcal{S}$, which gives us a unique signature of entanglement properties in many-body phases and dynamics [15], and is also of interest in the ongoing discussion on "quantum supremacy" [16–20].

Below, we will describe a protocol for measuring Rényi entropies $S^{(n)}(\rho_A)$ based on random measurements realized as random unitary operators applied to ρ_A and subsequent measurements of a fixed observable [21]. In our approach, the required random unitaries are implemented using the same atomic, molecular, and optical (AMO) toolbox which underlies the preparation of quantum phases and dynamics (cf. Fig. 1). This enables a physical implementation of the protocol, applicable to generic Hubbard and spin models and in arbitrary dimensions. We emphasize that, in contrast to recent protocols to measure nth order Rényi entropies, which requires the preparation of n identical copies [22–25], a random measurement protocol requires only a single

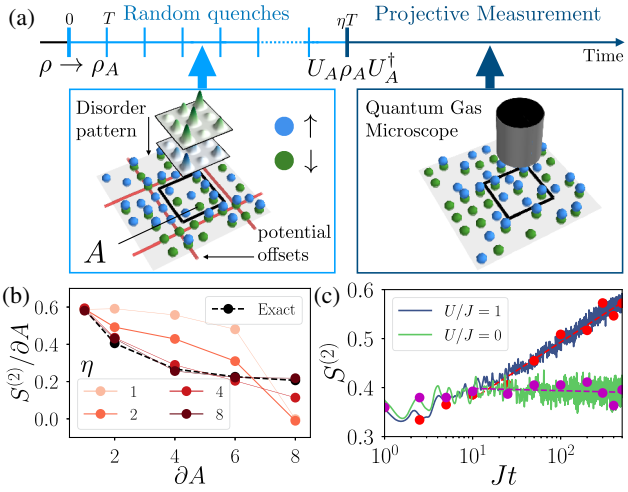

FIG. 1. Measuring Rényi entropies via random quenches. (a) Experimental sequence: For a given reduced density matrix $\rho_A = \mathrm{Tr}_{\mathcal{S}\setminus A}[\rho]$, we apply (i) a random unitary U_A realized by a series of η random quenches [cf. Eq. (3)], implemented using (spin-dependent) disorder potentials [cf. Eq. (4)]; this is followed by (ii) a projective measurement (readout) with a quantum gas microscope, to obtain $S^{(n)}(\rho_A)$ from Eq. (6). (b) Within our protocol, we illustrate for the ground state of a 2D Heisenberg model (8×8 sites) area law scaling of $S^{(2)} \propto \partial A$ (with ∂A the perimeter of area A), showing convergence with increasing η to the exact value (black line). (c) For the many-body localized phase of the 1D Bose-Hubbard model (ten sites and five particles), we illustrate a measurement of the logarithmic growth of $S^{(2)}(\rho_A)$ at half partition as a function of time. The exact value of $S^{(2)}(\rho_A)$ (solid lines) is compared to the estimated values (dots). The dashed lines are linear fits. The simulated experiments in (b) and (c) assume $N_U = 100$ random unitaries and $N_M = 100$ measurements per random unitary (see the text).

quantum system [21] and thus can be implemented directly with existing AMO and solid state platforms [26,27]. A central aspect in any measurement scheme for Rényi entropies, as for quantum state tomography [28–30], is scaling of the experimental effort with the size of the system of interest: Below, we provide a detailed analysis and feasibility study of the required resources in terms of the number of measurements and random unitaries and verification of random unitaries [31].

Random measurements to infer Rényi entropies have been discussed in a quantum information context [21]. These consist in applying to ρ_A a random unitary matrix U_A from the circular unitary ensemble (CUE) followed by a measurement in the fixed computational basis to access to the outcome probabilities $P(\mathbf{s}) = \mathrm{Tr}[U_A \rho_A U_A^\dagger \mathcal{P}_\mathbf{s}]$ with $\mathcal{P}_\mathbf{s} = |\mathbf{s}\rangle\langle\mathbf{s}|$ projectors onto the basis states $|\mathbf{s}\rangle$. The extraction of the Rényi entropies $S^{(n)}(\rho_A)$ is then based on the estimation of the statistical moments

$$\langle P(\mathbf{s})^n \rangle = \langle \mathrm{Tr}[(U_A \rho_A U_A^\dagger)^{\otimes n} \mathcal{P}_\mathbf{s}^{\otimes n}] \rangle, \tag{1}$$

with $\langle \ldots \rangle$ the ensemble average over random unitaries. In order to obtain $S^{(n)}(\rho_A)$ from Eq. (1), one relies on the statistical properties of the correlators between the matrix elements $u_{\mathbf{ij}}$ of U_A. In particular, for $n = 2$, one exploits the identity

$$\langle u_{\mathbf{s}i_1} u^*_{\mathbf{s}i_2} u_{\mathbf{s}i_3} u^*_{\mathbf{s}i_4} \rangle = \frac{\delta_{\mathbf{i}_1,\mathbf{i}_2}\delta_{\mathbf{i}_3,\mathbf{i}_4} + \delta_{\mathbf{i}_1,\mathbf{i}_4}\delta_{\mathbf{i}_2,\mathbf{i}_3}}{\mathcal{N}_A(\mathcal{N}_A+1)}, \tag{2}$$

with $\mathcal{N}_A$ the Hilbert space dimension of A, to obtain $\langle P(\mathbf{s})^2 \rangle = (1 + \mathrm{Tr}[\rho_A^2])/[\mathcal{N}_A(\mathcal{N}_A+1)]$ [21]. Inverting this relation warrants direct access to $S^{(2)}(\rho_A)$ as a function of $P(\mathbf{s})$ [32]. In the following, we use that the required identities of nth order correlators of the CUE are reproduced by unitary n designs [33,34], i.e., ensembles of random unitary matrices approximating the CUE by having the same correlators up to nth order [35]. In contrast to the seminal experiments measuring $S^{(2)}(\rho_A)$ in a Bose-Hubbard (BH) model [24] which rely on the preparation of physical copies of the quantum system [22], the present scheme works with single copies [21]: The moments (1) can be interpreted as a replica trick to create n virtual copies [cf. Eq. (1)]. We present additional details and a diagrammatic approach in Supplemental Material [36].

While in a quantum information context random unitaries from unitary n designs are generated as a sequence of random gates [21,43,44], we show that such random unitaries can be realized with the existing AMO toolbox, as a series of quenches in interacting Hubbard and spin models with engineered disorder:

$$U_A = e^{-iH_A^\eta T} \ldots e^{-iH_A^1 T}, \tag{3}$$

followed by a readout with a quantum gas microscope (see Fig. 1). Here, H_A^j denotes the Hamiltonian for a given disorder pattern j. In total, we consider η quenches of duration T, with $T_{\mathrm{tot}} \equiv \eta T$ the total time. The questions to be addressed are (i) the convergence to the CUE in terms of n designs [cf. Eq. (2)] with "depth" η, in view of experimentally available disorder Hamiltonians and experimental verification, and (ii) the scaling of statistical errors with the number of applied random unitaries N_U and the number of measurements per random unitary N_M. We emphasize the relation of (i) to the ongoing theoretical [39–41,45,46] and experimental [47] investigation of thermalization dynamics of periodically driven quantum systems and their connection to quantum chaos [48]. The type of problems which can be addressed with our protocol are illustrated in Figs. 1(b) and 1(c), with the simulation of the measurement of an area law for a 2D-Heisenberg model [49] and of the entropy growth in many-body localized (MBL) [50–54] dynamics in the BH model, with details on the simulations presented below and in Supplemental Material [36].

Protocol for the Fermi-Hubbard model.—In view of recent progress in realizing the 2D Fermi-Hubbard (FH) model [5–8], we wish to illustrate the protocol for spinful fermions in a 2D optical lattice [cf. Fig. 1(a)]. The FH Hamiltonian is

$$H_F = -t_F \sum_{\langle \mathbf{i},\mathbf{l}\rangle \in \mathcal{S},\sigma} c^\dagger_{\mathbf{i}\sigma} c_{\mathbf{l}\sigma} + U \sum_{\mathbf{i}\in\mathcal{S}} n_{\mathbf{i}\uparrow} n_{\mathbf{i}\downarrow} \tag{4}$$

with hopping amplitude t_F and interaction strength U. Here $c^{(\dagger)}_{\mathbf{i},\sigma}$ denote fermionic annihilation (creation) operators at lattice site $\mathbf{i} = (i_x, i_y)$ and spin $\sigma \in \{\uparrow,\downarrow\}$, and $n_{\mathbf{i}\sigma} = c^\dagger_{\mathbf{i}\sigma} c_{\mathbf{i}\sigma}$. We will add disorder below to realize H_A^j.

We assume that the (non)equilibrium quantum many-body state ρ of interest has been prepared in the full system $\mathcal{S}$. The experimental sequence to measure Rényi entropies $S^{(n)}(\rho_A)$ of the reduced density matrix $\rho_A = \mathrm{Tr}_{\mathcal{S}\setminus A}[\rho]$ is shown in Fig. 1(a): (i) Isolation of the partition A of dimension (L_x, L_y) and $L \equiv L_x L_y$ the number of isolated sites is obtained via spatial addressing [cf. Fig. 1(a)]. The Hamiltonian H_A^j is realized as restriction $H_A^j = H_F|_A + \sum_{\mathbf{i}\in A,\sigma} \delta^j_{\mathbf{i},\sigma} n_{\mathbf{i}\sigma}$ with random lattice offsets $\delta^j_{\mathbf{i},\sigma}$. Because of particle and spin conservation in H_F, U_A decomposes into blocks with different particle numbers N and magnetization S_z, $U_A = \bigoplus_{N,S_z} U_A^{(N,S_z)}$ and $\rho_A = \bigoplus_{N,S_z} \rho_A^{(N,S_z)}$. Below, we study in each block the realization of a random unitary $U_A^{(N,S_z)}$ from an n design ($n = 2, 3, \ldots$) as a function of η and T_{tot}. (ii) Lattice site occupations $\mathbf{s}_{N,S_z}$ are measured with a quantum gas microscope, where $\mathbf{s}_{N,S_z} = (n_{\mathbf{i},\uparrow}, n_{\mathbf{i},\downarrow})_\mathbf{i}$ determines $N = \sum_{\mathbf{i}\in A}(n_{\mathbf{i}\uparrow} + n_{\mathbf{i}\downarrow})$ and $S_z = \sum_{\mathbf{i}\in A}(n_{\mathbf{i}\uparrow} - n_{\mathbf{i}\downarrow})$. By repeating steps (i) and (ii) with the same U_A, i.e., the same series of random quenches, to perform N_M measurements, one estimates the probabilities $P(\mathbf{s}_{N,S_z}) = \mathrm{Tr}[U_A \rho_A U_A^\dagger \mathcal{P}_{\mathbf{s}_{N,S_z}}]$

with $\mathcal{P}_{\mathbf{s}_{N,S_z}}$ the projector onto the Fock state $|\mathbf{s}_{N,S_z}\rangle$ [55]. Repeating this for N_U different unitaries, we estimate the ensemble averages $\langle P(\mathbf{s}_{N,S_z})^n\rangle$, related to functionals of ρ_A [21]. Using 1- and 2-design properties, we find

$$\langle P(\mathbf{s}_{N,S_z})\rangle = \frac{\mathrm{Tr}[\rho_A^{(N,S_z)}]}{\mathcal{N}_A^{(N,S_z)}}, \tag{5}$$

$$\langle P(\mathbf{s}_{N,S_z})^2\rangle = \frac{\mathrm{Tr}[\rho_A^{(N,S_z)}]^2 + \mathrm{Tr}[\rho_A^{(N,S_z)2}]}{\mathcal{N}_A^{(N,S_z)}(\mathcal{N}_A^{(N,S_z)}+1)}, \tag{6}$$

where $\mathcal{N}_A^{(N,S_z)}$ is the Hilbert space dimension of the particle-spin block in the subsystem A. Hence, from estimations of $\langle P(\mathbf{s}_{N,S_z})^n\rangle$ $(n = 1, 2)$, $\mathrm{Tr}[\rho_A^{(N,S_z)2}]$ can be extracted. By summation over all blocks, one obtains the total purity $p_2 \equiv \mathrm{Tr}[\rho_A^2] = \sum_{N,S_z}\mathrm{Tr}[\rho_A^{(N,S_z)2}]$ and finally $S^{(2)}(\rho_A)$. Higher-order ensemble averages $\langle P(\mathbf{s}_{N,S_z})^n\rangle$ are related to higher-order powers $\mathrm{Tr}(\rho_A^{(N,S_z)n})$ [31].

Generation of random unitaries.—Below, we present a numerical study of the generation of approximate unitary 2-designs [56–59], focusing on the convergence of the U_A [cf. Eq. (3)] to the CUE as a function of time $T_{\mathrm{tot}} = \eta T$ and depth η of the "random circuit." While the full system $\mathcal{S}$ can be arbitrary large, we emphasize that—in view of the scaling of statistical errors with the partition size A (see below)—the applicability of the protocol in an actual experiment will *a priori* be limited to domains A of moderate size, which can be simulated numerically. Here, we present results for the Heisenberg model in 1D and 2D, which allows larger partition sizes, and we refer to Ref. [31] for the FH model. The Hamiltonian is $H_h = J\sum_{\langle \mathbf{il}\rangle}\boldsymbol{\sigma}_\mathbf{i}.\boldsymbol{\sigma}_\mathbf{l}$, as obtained from Eq. (4) in the limit $U \gg t_F$ at half filling (alternatively with Rydberg atoms [60] or trapped ions [61]). Here, $\sigma_\mathbf{i}$ are the Pauli matrices, and $J = t_F^2/U$. To realize random quenches, we consider disorder potentials $\delta_\mathbf{i}^j = \delta_{\mathbf{i}\uparrow}^j - \delta_{\mathbf{i}\downarrow}^j$ drawn for each quench j from a normal distribution with standard deviation δ, i.e., $H_A^j \equiv H_h|_A + \sum_{\mathbf{i}\in A}\delta_\mathbf{i}^j\sigma_\mathbf{i}^z$ [62].

Figure 2 shows the error of the estimated purity $(p_2)_e$ of various test states ρ_A (defined in the caption) for partitions A of various sizes L in 1D $(L = L_x)$ and 2D $(L = L_xL_y)$ [64]. According to Figs. 2(a)–2(c), for a fixed quench time $JT = 1$ and disorder strength $\delta = J$, the error decreases exponentially with growing $JT_{\mathrm{tot}}/L = \eta/L$ towards a plateau, which corresponds to the statistical error threshold (see below). Thus, our results indicate "efficient" convergence of U_A to an approximate 2-design, after a total time T_{tot} which scales linearly with L, as in conventional random circuits based on engineered gates [56–58]. Note that our simulations show that product states, which are prepared in an experiment with high fidelity, provide good indicators of the convergence of the generated unitaries.

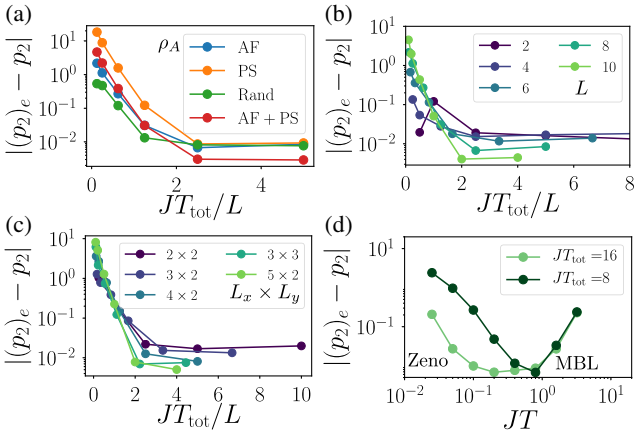

FIG. 2. Creation of approximate 2-designs in the Heisenberg model. (a) Average error of the estimated purity $|(p_2)_e - (p_2)|$ for a unidimensional partition of size $L = 8$ and various test states: an antiferromagnetic state $|\psi_{\mathrm{AFM}}\rangle$, the phase separated state $|\psi_{\mathrm{PS}}\rangle = \prod_{\mathbf{i},i_x\le L_x/2}|\downarrow\rangle_\mathbf{i}\prod_{\mathbf{i},i_x>L_x/2}|\uparrow\rangle_\mathbf{i}$, a pure random state $|\psi_{\mathrm{rand}}\rangle$ with $S_z = 0$, and the mixed state $\rho_A = \frac{1}{2}(|\psi_{\mathrm{AFM}}\rangle\langle\psi_{\mathrm{AFM}}| + |\psi_{\mathrm{PS}}\rangle\langle\psi_{\mathrm{PS}}|)$. (b),(c) Error for $\rho_A = |\psi_{\mathrm{AFM}}\rangle\langle\psi_{\mathrm{AFM}}|$ for (b) unidimensional partitions $(L = L_x)$ and (c) two-dimensional partitions $(L = L_xL_y)$. (d) Optimization of the quench time JT for fixed total time T_{tot} and disorder strength $\delta = J$. For all panels, we average over $N_U = 500$ unitaries and consider $N_M = \infty$.

For a given total time T_{tot}, set in an experiment by the finite coherence time, we show in Fig. 2(d) the existence of an optimal quench time $JT \approx 1$ to minimize errors. This reflects the trade-off between the requirements (i) to evolve the system for each quench j during a time sufficiently large compared to time scales J^{-1}, δ^{-1} set by the Hamiltonian [65], i.e., to prevent a quantum Zeno effect, and (ii) to change the disorder pattern frequently to prevent localization. There also exists an optimal disorder strength $\delta \approx J$ [36], resulting from a trade-off between localizing effects in the limit $\delta \gg J$ and a vanishing random component of the applied quenches in the limit $\delta \ll J$. We note that the use of a single disorder pattern, combined with random quench times $T \to T_j$, represents another possibility to generate the required random unitaries [36].

Our findings, in particular, the convergence to approximate 2-designs and the corresponding scalings, also apply to generic Fermi- and Bose-Hubbard models and quantum Ising models [31]. Moreover, we emphasize that (i) our measurement scheme does not rely on the knowledge of the applied unitaries U_A and (ii)—with respect to state-of-the-art AMO setups—the measurement protocol is robust against imperfect reproducibility of the generated unitaries, finite detection fidelity, and decoherence [31]. While we are interested in this work in the limit of large times T_{tot} where approximate 2-designs are created (as part of our measurement scheme), we finally remark that random quenches in AMO systems provide a platform to study fast thermalization dynamics towards quantum chaos [31] and

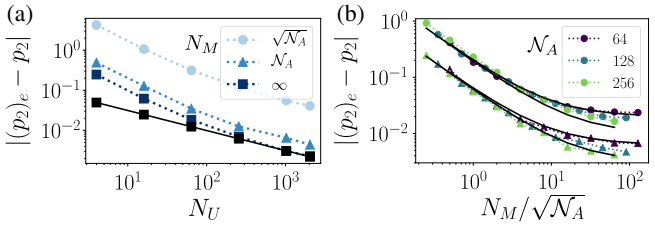

FIG. 3. Scaling of statistical errors. (a) Average statistical error of the estimated purity as a function of N_U for various N_M, $\mathcal{N}_A = 256$. (b) Error as a function of N_M, for different $\mathcal{N}_A$, showing birthday paradox scaling $N_M/\sqrt{\mathcal{N}_A}$. Circles represent $N_U = 100$ and triangles $N_U = 1000$. The unitaries are sampled from the CUE numerically [42]. The black lines represent the expressions given in the text and Ref. [31].

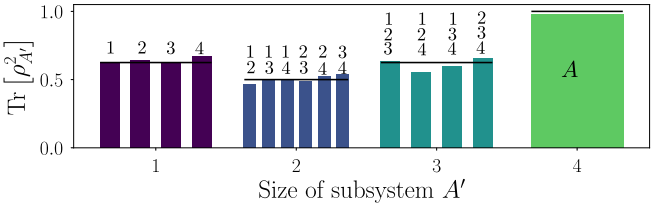

FIG. 4. Protocol with local unitaries. Purity of all (sub)systems $A' \subseteq A$ with $N_U = 2N_M = 100$. The numbers refer to the indices $i = 1, \ldots, L$ contained in A', the green bar to $A' = A$. The black lines indicate the exact values.

the entanglement growth associated with random time evolution [66].

Statistical errors.—We now discuss the statistical errors due to a finite number of random unitaries N_U and of measurements N_M per unitary. For simplicity, we assume that $\rho_A = \rho_A^{(N,S_z)}$ describes a state in a single spin-particle sector with dimension $\mathcal{N}_A^{(N,S_z)}$, where random unitaries from the CUE are created. Since the following discussion is not specific to an underlying model, we also drop the labels (N, S_z). In Fig. 3(a), the average error of the purity is shown as a function of N_U, decreasing as $1/\sqrt{N_U}$ for fixed N_M. In Fig. 3(b), it is represented as a function of N_M, for $N_U = 100$ and 1000. We find that, for $N_U \gg 1$, the error scales as $|(p_2)_e - p_2| \sim (C_2 + \mathcal{N}_A/N_M)/\sqrt{\mathcal{N}_A N_U}$, where $C_2 = \mathcal{O}(1)$ is largest for pure states. The results are confirmed by the analytical study presented in Ref. [31]. The first term, independent of N_M, arises from the finite value of N_U [21]. The second originates from the finite number N_M of measurements. It leads to a requirement of $N_M \sim \sqrt{\mathcal{N}_A}$ to determine the purity up to an error of the order $1/\sqrt{N_U}$. This scaling is directly related to the statistics of doublons obtained when sampling a discrete variable (the birthday paradox [67]).

The total number of measurements $N_M N_U$ scales polynomially with the Hilbert space dimension $\mathcal{N}_A$ and thus exponentially with the size of A (independently of the total system $\mathcal{S}$). However, compared to quantum state tomography, the exponent is favorable and allows us to perform measurements of $S^{(2)}(\rho_A)$ for subsystem sizes, which are, for instance, compatible with the examples in Fig. 1.

Application to physical examples.—We conclude our discussion by presenting applications of the protocol investigating entanglement properties of quantum many-body states $|\psi\rangle$. As a first example, we demonstrate in Fig. 1(b) the measurement of an area law in a 2D Heisenberg model. We consider a system $\mathcal{S}$ prepared in the $S_z = 0$ ground state $|\psi\rangle$ of H_h on an 8×8 square lattice, obtained numerically with the density matrix renormalization group (DMRG) [68]. For rectangular partitions A with size $L = L_x L_y$ placed at the center of the system, we estimate the second Rényi entropy $S^{(2)}(\rho_A)$ of the reduced density matrices $\rho_A = \mathrm{Tr}_{\mathcal{S}\setminus A}[|\psi\rangle\langle\psi|]$ as a function of the partition boundary $\partial A = 2(L_x + L_y - 2)$. We observe that the estimated Rényi entropy converges to the area law result [49] with an increasing number of quenches η. The quench parameters are $\delta = J = 1/T$. Note that we have used here a finite number of unitaries $N_U = 100$ and a finite number of measurements $N_M = 100$. As second example, Fig. 1(c) shows for a 1D Bose-Hubbard model the entanglement growth in the MBL phase [51,52], with details on the model and parameters summarized in Supplemental Material [36]. According to Fig. 1(c), the estimated second-order Rényi entropy as a function of time clearly allows us to distinguish MBL from Anderson localization.

Protocol based on local unitaries.—The measurement scheme described above relies on global entangling unitaries acting on the entire Hilbert space. As an alternative, we can use local unitaries, which act individually on local constituents $i = 1, \ldots, L$ (e.g., spins) of A. Here, the unitary U_A is given as a product $U_A = u_1 \otimes \cdots \otimes u_L$, where each u_i is independently drawn from a unitary 2-design in the local Hilbert space of dimension d. In the case of a spin system, the u_i can be viewed as a random single spin rotation on the Bloch sphere. As above, from measurements of the local spin configuration with outcome $\mathbf{s} = (s_i)_{i=1,\ldots,L}$, we compute the statistical moments $\langle P(\mathbf{s})^n \rangle$. We find $\langle P(\mathbf{s}) \rangle = 1/d^L$ [69] and, using the 2-design properties of u_i,

$$\langle P(\mathbf{s})^2 \rangle = \frac{\sum_{A' \subseteq A} \mathrm{Tr}(\rho_{A'}^2)}{d^L (d+1)^L}. \tag{7}$$

Here, we sum over all subsystems $A' \subseteq A$, including the empty subsystem with $\mathrm{Tr}[\rho_\varnothing^2] \equiv 1$. Since the unitaries act only locally, Eq. (7) holds for each subsystem A'. This allows us to reconstruct recursively all purities $\mathrm{Tr}(\rho_{A'}^2)$ for $A' \subseteq A$. Local unitaries thus allow us to infer more information from the measurement than global unitaries. This is illustrated in Fig. 4 for $L = 4$ spins initialized in the W state. We note, however, that, due to the recursive reconstruction of the purities from Eq. (7), this protocol is more prone to statistical errors [36].

Conclusion and outlook.—Our protocol allows the measurement of Rényi entropies based on single copies in existing AMO setups: For example, to obtain the purity of ρ_A of a partition A with $L = 14$ spins, as part of an arbitrarily large many-body system, one needs for an accuracy of $\sim 5\%$ to create unitaries during a time $JT_{\mathrm{tot}} \sim 25$ and to perform $N_M = 500$ measurements for $N_U = 100$ unitaries. While we have focused on the measurement of second-order Rényi entropies, higher-order entropies are also accessible although with increasing statistical errors [31], which provides an interesting perspective to extend the protocol to von Neumann entropies or the entanglement spectrum [70–72].

We thank the M. Lukin, M. Greiner, M. Hafezi group members and J. Eisert, C. Roos, P. Jurcevic, G. Pagano, W. Lechner, M. Baranov, H. Pichler, P. Hauke, M. Łącki, and D. Hangleiter for discussions. The DMRG and exact diagonalization simulations were performed using the ITensor library [73] and QuTiP [74], respectively. Work in Innsbruck is supported by the ERC Synergy Grant UQUAM and the SFB FoQuS (FWF Project No. F4016-N23). J. I. C. acknowledges support from the ERC grant QUENOCOBA.

A. E. and B. V. contributed equally to this work.

[1] I. Bloch, J. Dalibard, and S. Nascimbène, Nat. Phys. **8**, 267 (2012).
[2] A. Browaeys, D. Barredo, and T. Lahaye, J. Phys. B **49**, 152001 (2016).
[3] R. Blatt and C. F. Roos, Nat. Phys. **8**, 277 (2012).
[4] S. Murmann, A. Bergschneider, V. M. Klinkhamer, G. Zürn, T. Lompe, and S. Jochim, Phys. Rev. Lett. **114**, 080402 (2015).
[5] E. Haller, J. Hudson, A. Kelly, D. A. Cotta, B. Peaudecerf, G. D. Bruce, and S. Kuhr, Nat. Phys. **11**, 738 (2015).
[6] D. Greif, M. F. Parsons, A. Mazurenko, C. S. Chiu, S. Blatt, F. Huber, G. Ji, and M. Greiner, Science **351**, 953 (2016).
[7] M. Boll, T. A. Hilker, G. Salomon, A. Omran, J. Nespolo, L. Pollet, I. Bloch, and C. Gross, Science **353**, 1257 (2016).
[8] L. W. Cheuk, M. A. Nichols, K. R. Lawrence, M. Okan, H. Zhang, E. Khatami, N. Trivedi, T. Paiva, M. Rigol, and M. W. Zwierlein, Science **353**, 1260 (2016).
[9] H. Labuhn, D. Barredo, S. Ravets, S. de Léséleuc, T. Macrì, T. Lahaye, and A. Browaeys, Nature (London) **534**, 667 (2016).
[10] J. Zeiher, J.-y. Choi, A. Rubio-Abadal, T. Pohl, R. M. W. van Bijnen, I. Bloch, and C. Gross, Phys. Rev. X **7** 041063 (2017).
[11] H. Bernien, S. Schwartz, A. Keesling, H. Levine, A. Omran, H. Pichler, S. Choi, A. S. Zibrov, M. Endres, M. Greiner, V. Vuletić, and M. D. Lukin, Nature (London) **551**, 579 (2017).
[12] P. Jurcevic, H. Shen, P. Hauke, C. Maier, T. Brydges, C. Hempel, B. P. Lanyon, M. Heyl, R. Blatt, and C. F. Roos, Phys. Rev. Lett. **119**, 080501 (2017).
[13] J. Zhang, G. Pagano, P. W. Hess, A. Kyprianidis, P. Becker, H. Kaplan, A. V. Gorshkov, Z. X. Gong, and C. Monroe, Nature **551**, 601 (2017).
[14] S. Kuhr, Natl. Sci. Rev. **3**, 170 (2016).
[15] J. Eisert, M. Cramer, and M. B. Plenio, Rev. Mod. Phys. **82**, 277 (2010).
[16] S. Boixo, S. V. Isakov, V. N. Smelyanskiy, R. Babbush, N. Ding, Z. Jiang, M. J. Bremner, J. M. Martinis, and H. Neven, arXiv:1608.00263.
[17] J. Bermejo-Vega, D. Hangleiter, M. Schwarz, R. Raussendorf, and J. Eisert, arXiv:1703.00466.
[18] X. Gao, S. T. Wang, and L. M. Duan, Phys. Rev. Lett. **118**, 040502 (2017).
[19] M. J. Bremner, A. Montanaro, and D. J. Shepherd, Quantum Topol. **1**, 8 (2017).
[20] S. Boixo, V. N. Smelyanskiy, and H. Neven, arXiv:1708.01875.
[21] S. J. van Enk and C. W. J. Beenakker, Phys. Rev. Lett. **108**, 110503 (2012).
[22] A. J. Daley, H. Pichler, J. Schachenmayer, and P. Zoller, Phys. Rev. Lett. **109**, 020505 (2012).
[23] D. A. Abanin and E. Demler, Phys. Rev. Lett. **109**, 020504 (2012).
[24] R. Islam, R. Ma, P. M. Preiss, M. Eric Tai, A. Lukin, M. Rispoli, and M. Greiner, Nature (London) **528**, 77 (2015).
[25] A. M. Kaufman, M. E. Tai, A. Lukin, M. Rispoli, R. Schittko, P. M. Preiss, and M. Greiner, Science **353**, 794 (2016).
[26] A. a. Houck, H. E. Türeci, and J. Koch, Nat. Phys. **8**, 292 (2012).
[27] J. Cai, A. Retzker, F. Jelezko, and M. B. Plenio, Nat. Phys. **9**, 168 (2013).
[28] D. Gross, Y.-k. Liu, S. T. Flammia, S. Becker, and J. Eisert, Phys. Rev. Lett. **105**, 150401 (2010).
[29] M. Cramer, M. B. Plenio, S. T. Flammia, R. Somma, D. Gross, S. D. Bartlett, O. Landon-Cardinal, D. Poulin, and Y.-K. Liu, Nat. Commun. **1**, 149 (2010).
[30] B. P. Lanyon, C. Maier, M. Holzäpfel, T. Baumgratz, C. Hempel, P. Jurcevic, I. Dhand, A. S. Buyskikh, A. J. Daley, M. Cramer, M. B. Plenio, R. Blatt, and C. F. Roos, Nat. Phys.
[31] For details, see the companion paper: B. Vermersch, A. Elben, M. Dalmonte, J. I. Cirac, and P. Zoller, Phys. Rev. A **97**, 023604 (2018).
[32] By averaging estimated $S^{(2)}(\rho_A)$ obtained from different states $\mathbf{s}$, statistical errors are reduced (cf. below).
[33] D. Gross, K. Audenaert, and J. Eisert, J. Math. Phys. (N.Y.) **48**, 052104 (2007).
[34] A. Roy and A. J. Scott, Des. Codes Cryptogr. **53**, 13 (2009).
[35] For example, Eq. (2) is satisfied for 2-designs.
[36] See Supplemental Material at http://link.aps.org/supplemental/10.1103/PhysRevLett.120.050406 for a diagrammatic approach to random measurements, and additional details on the physical examples and simulations, which includes Refs. [37–42].
[37] J. Gray, L. Banchi, A. Bayat, and S. Bose, arXiv:1709.04923.
[38] B. Collins and I. Nechita, Commun. Math. Phys. **297**, 345 (2010).
[39] L. D'Alessio and A. Polkovnikov, Ann. Phys. (Berlin) **333**, 19 (2013).

[40] L. D'Alessio and M. Rigol, Phys. Rev. X **4**, 041048 (2014).
[41] F. Machado, G. D. Meyer, D. V. Else, C. Nayak, and N. Y. Yao, arXiv:1708.01620.
[42] F. Mezzadri, Not. Am. Math. Soc. **54**, 592 (2006).
[43] R. Oliveira, O. C. O. Dahlsten, and M. B. Plenio, Phys. Rev. Lett. **98**, 130502 (2007).
[44] M. Žnidarič, Phys. Rev. A **78**, 032324 (2008).
[45] P. Ponte, A. Chandran, Z. Papić, and D. A. Abanin, Ann. Phys. (Berlin) **353**, 196 (2015).
[46] S. Gopalakrishnan, M. Knap, and E. Demler, Phys. Rev. B **94**, 094201 (2016).
[47] P. Bordia, H. Lüschen, U. Schneider, M. Knap, and I. Bloch, Nat. Phys. **13**, 460 (2017).
[48] F. Haake, *Quantum Signatures of Chaos* (Springer, New York, 2010), Vol. 54.
[49] H. F. Song, N. Laflorencie, S. Rachel, and K. Le Hur, Phys. Rev. B **83**, 224410 (2011).
[50] D. M. Basko, I. L. Aleiner, and B. L. Altshuler, Ann. Phys. (Berlin) **321**, 1126 (2006).
[51] J. H. Bardarson, F. Pollmann, and J. E. Moore, Phys. Rev. Lett. **109**, 017202 (2012).
[52] M. Serbyn, Z. Papić, and D. A. Abanin, Phys. Rev. Lett. **110**, 260601 (2013).
[53] R. Nandkishore and D. A. Huse, Annu. Rev. Condens. Matter Phys. **6**, 15 (2015).
[54] E. Altman and R. Vosk, Annu. Rev. Condens. Matter Phys. **6**, 383 (2015).
[55] Our protocol can be realized with other observables [31].
[56] C. Dankert, R. Cleve, J. Emerson, and E. Livine, Phys. Rev. A **80**, 012304 (2009).
[57] M. Ohliger, V. Nesme, and J. Eisert, New J. Phys. **15**, 015024 (2013).
[58] F. Brandão, A. W. Harrow, and M. Horodecki, Commun. Math. Phys. **346**, 397 (2016).
[59] L. Banchi, D. Burgarth, and M. J. Kastoryano, Phys. Rev. X **7**, 041015 (2017).
[60] A. V. Gorshkov, S. R. Manmana, G. Chen, E. Demler, M. D. Lukin, and A. M. Rey, Phys. Rev. A **84**, 033619 (2011).
[61] D. Porras and J. I. Cirac, Phys. Rev. Lett. **92**, 207901 (2004).
[62] We have found that random unitaries can be realized using Aubry-André potentials [63] with similar convergence times.
[63] S. Aubry and G. André, Ann. Isr. Phys. Soc. **3**, 133 (1980).
[64] Note that $(p_2)_e$ can be larger than 1 when $T_{\mathrm{tot}} \to 0$.
[65] P. Facchi, S. Montangero, R. Fazio, and S. Pascazio, Phys. Rev. A **71**, 060306 (2005).
[66] A. Nahum, J. Ruhman, S. Vijay, and J. Haah, Phys. Rev. X **7**, 031016 (2017).
[67] S. M. Blinder, *Guide to Essential Math: A Review for Physics*, Chemistry and Engineering Students (Elsevier, New York, 2013).
[68] With maximal bond dimension 4000 and 17 sweeps.
[69] The unitaries U_A form a 1-design.
[70] H. Li and F. D. M. Haldane, Phys. Rev. Lett. **101**, 010504 (2008).
[71] H. Pichler, G. Zhu, A. Seif, P. Zoller, and M. Hafezi, Phys. Rev. X **6**, 041033 (2016).
[72] M. Dalmonte, B. Vermersch, and P. Zoller, arXiv:1707.04455.
[73] http://itensor.org.
[74] J. R. Johansson, P. D. Nation, and F. Nori, Comput. Phys. Commun. **184**, 1234 (2013).